School of Natural Sciences and Mathematics

Fast Magnetosonic Waves Observed by Van Allen Probes: Testing Local Wave Excitation Mechanism—Supplement

UT Dallas Author(s):

Lunjin Chen

Citation:

Min, K., Liu, K., Wang, X., Chen, L., and Denton, R. E. 2018. "Fast magnetosonic waves observed by Van Allen Probes: Testing local wave excitation mechanism." Journal of Geophysical Research: Space Physics 123(1): 497– 512, doi:10.1002/2017JA024867

Supporting Information for "Fast magnetosonic waves observed by Van Allen Probes: Testing local wave excitation mechanism"

Kyungguk Min[1], Kaijun Liu[2], Xueyi Wang[2], Lunjin Chen[3], Richard E. Denton[4]

Contents of this file

1. Text S1

Corresponding author: K. Min, Johns Hopkins University Applied Physics Laboratory, Laurel, Maryland, USA. (Kyungguk.Min@jhuapl.edu)

[1]Johns Hopkins University Applied Physics Laboratory, Laurel, Maryland, USA.

[2]Department of Physics, Auburn University, Auburn, Alabama, USA.

[3]Department of Physics, University of Texas at Dallas, Richardson, Texas, USA.

[4]Department of Physics and Astronomy, Dartmouth College, Hanover, New Hampshire, USA.

2. Figures S1 to S5

Introduction Text S1 provides the linear theory analysis investigating the potential effect of suprathermal electrons measured by the spacecraft but not used in the simulations. Figure S1 shows frequency power spectra of both electric and magnetic field fluctuations measured from the burst-mode data. Figures S2 and S3 show the linear theory results for the proton-to-electron mass ratios $m_p/m_e = 100$ and 225, respectively. Figure S4 shows the summary of the PIC simulation with $m_p/m_e = 100$. Figure S5 supports the analysis in Text S1.

Text S1. *Horne et al.* [2000] showed that thermal and suprathermal electrons can affect the ion Bernstein instability through Landau resonance. In the simulations presented in the article, however, the electrons were represented by a single Maxwellian with $\beta_e = 0.01$ (equivalent to $T_e = 17.7$ eV) for simplicity and to reduce simulation costs because the electron measurement accounts for only $\lesssim 1\%$ of the total electron density derived from the upper hybrid frequency line. This section uses linear theory and the measured electron phase space density to show that this simplified assumption will not alter the essential conclusion of the article.

Figure S5a shows the electron phase space density as a function of energy at all measured pitch angle bins. Similar to the proton case, the electron data are averaged in time to enhance the statistics. In general, the energy spectra are fairly smooth, monotonically decreasing and harder than a Maxwellian. Although there are variations in pitch angle space, we assume a pitch angle isotropy for simplicity. The black curve is a fit using two isotropic kappa distributions, each of which has the form

$$f_j = \frac{n_j}{\pi^{3/2}\theta_j^3} \frac{\Gamma(\kappa_j)}{\sqrt{\kappa_j}\Gamma(\kappa_j - 0.5)} \left(1 + \frac{v^2}{\kappa_j \theta_j^2}\right)^{-(\kappa_j+1)}, \tag{1}$$

where $\kappa_j > 3/2$ is the power index and $\Gamma(x)$ is the gamma function [e.g., *Summers and Thorne*, 1991]. The effective temperature then reads $T_j/m_j\theta_j^2 = \kappa_j/(2\kappa_j - 3)$. The fitting parameters are $n_j/n_e = 0.0376$ and $T_j = 8.68$ eV for the first component, and $n_j/n_e = 0.00226$ and $T_j = 1.87$ keV for the second component. And for both components, we choose $\kappa_j = 2$. Because about 96% of the total electrons are not captured by the instrument, we assume that the background electrons have a Maxwellian distribution with a temperature 1.77 eV.

Proton Model 2 with this kappa electron model is used to solve the dispersion relation. (The dielectric tensor elements for the kappa distribution of equation (1) are given by *Summers et al.* [1994].) In Figures S5b–S5d, growth rates obtained at $k_\parallel c/\omega_{pp} = 0.05$, 0.6 and 0.95 are compared with those of proton Model 2 combined with the single-Maxwellian electron model in the article. For $k_\parallel c/\omega_{pp} = 0.05$, the difference is negligible except for the very high frequency modes. For $k_\parallel c/\omega_{pp} = 0.6$ and 0.95, however, almost all harmonics experience damping by at most $0.01\Omega_p$. Nevertheless, the damping by the suprathermal electrons is less than 10% of the maximum growth rate of $\sim 0.15\Omega_p$, most likely owing to the small concentration of the suprathermal electrons. Interestingly, the damping is more effective at large $k_\parallel$. This suggests that the suprathermal electrons, if sufficiently dense, can further suppress the half harmonic modes at $k_\parallel c/\omega_{pp} \approx 0.6$ and the continuous mode at larger $k_\parallel$, thereby resulting in sharper full harmonic modes in the frequency spectrum of the simulated electric and magnetic field fluctuations.

References

Horne, R. B., G. V. Wheeler, and H. S. C. K. Alleyne (2000), Proton and electron heating by radially propagating fast magnetosonic waves, *Journal of Geophysical Research (Space Physics)*, *105*, 27,597–27,610, doi:10.1029/2000JA000018.

Summers, D., and R. M. Thorne (1991), The modified plasma dispersion function, *Physics of Fluids B*, *3*, 1835–1847, doi:10.1063/1.859653.

Summers, D., S. Xue, and R. M. Thorne (1994), Calculation of the dielectric tensor for a generalized Lorentzian (kappa) distribution function, *Physics of Plasmas*, *1*, 2012–2025, doi:10.1063/1.870656.

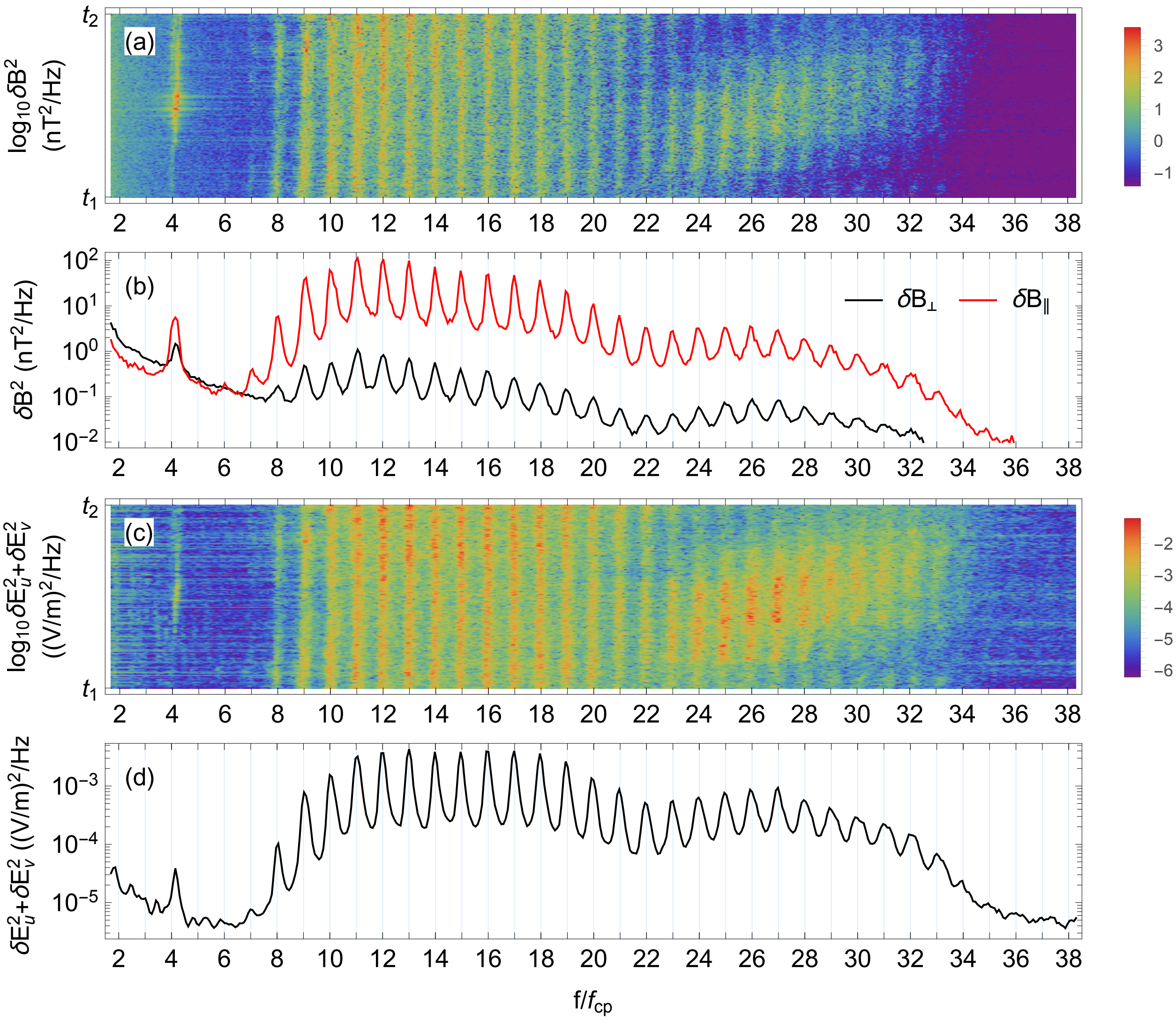

Figure S1. Magnetic and electric field frequency power spectra from the EMFISIS burst-mode waveforms. (a) shows $|\delta\mathbf{B}|^2 = |\delta B_U|^2 + |\delta B_V|^2 + |\delta B_W|^2$ as a function of time (vertical axis) and frequency normalized to the local proton cyclotron frequency (bottom axis). (b) shows log averages of the compressional (red) and transverse (black) components of the magnetic field frequency power spectrum. (c) shows $|\delta E_U|^2 + |\delta E_V|^2$ (without the spin component). (d) shows log average of $|\delta E_U|^2 + |\delta E_V|^2$. The time t_1 and t_2 in the vertical axes of (a) and (c) denote 2130 and 2150 UT, respectively.

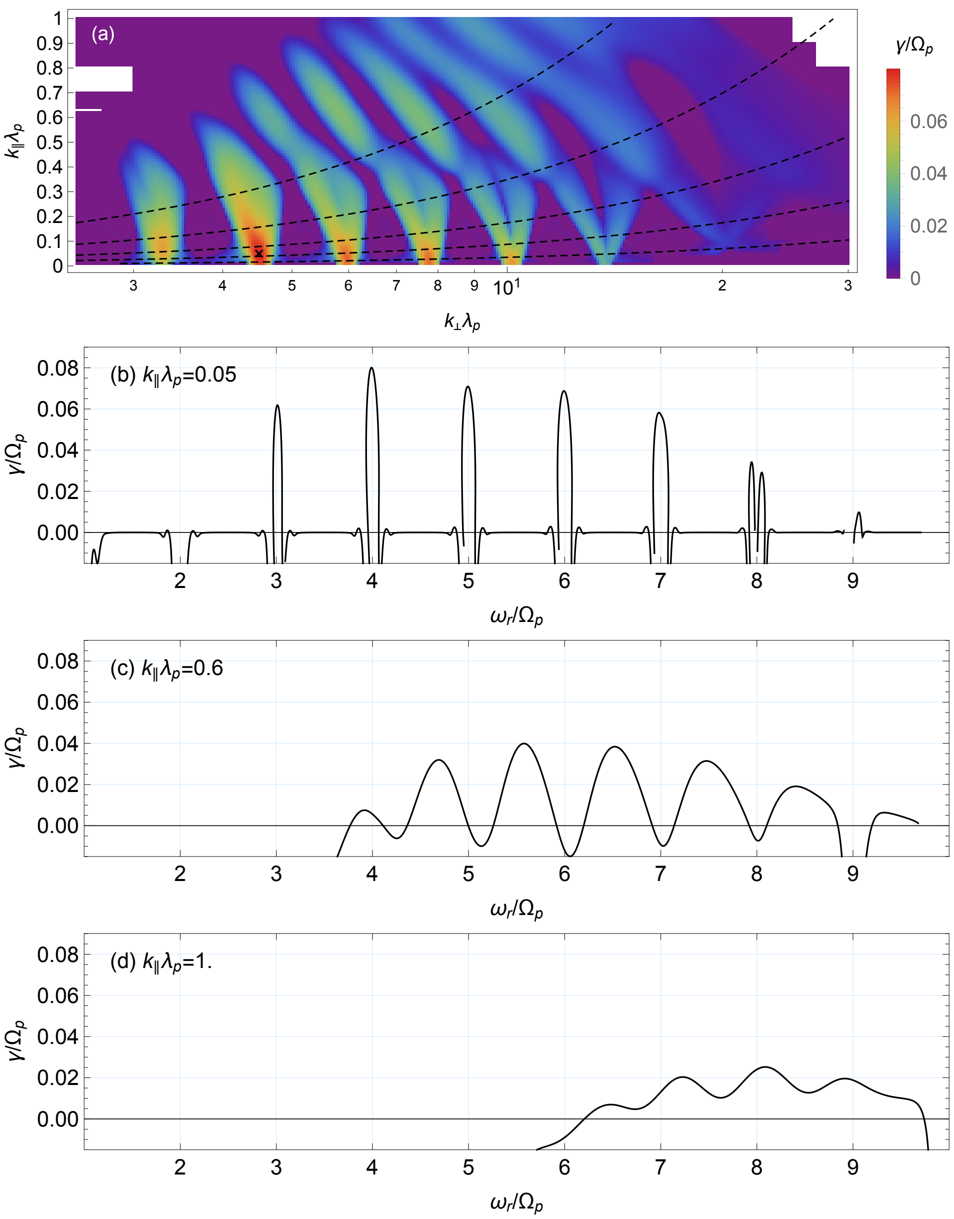

Figure S2. Linear theory results of the ion Bernstein instability for $m_p/m_e = 100$ and for Model 2 (see Table 1 in the article). (a) Linear growth rates as a function of parallel and perpendicular wave numbers normalized to the proton inertial length, $\lambda_p \equiv c/\omega_{pp}$. The cross symbol locates the fastest linear growth. The dashed curves denote constant wave normal angle contours (from top to bottom, 86°, 88°, 89°, 89.5° and 89.8°, respectively). Deep purple color denotes $\gamma/\Omega_p \leq 0$, and white patches are the regions not covered or where no solutions were found. (b, c, and d) Linear growth rates as a function of real frequency normalized to the proton cyclotron frequency at $k_\parallel \lambda_p =$ (b) 0.05, (c) 0.6 and (d) 1, respectively.

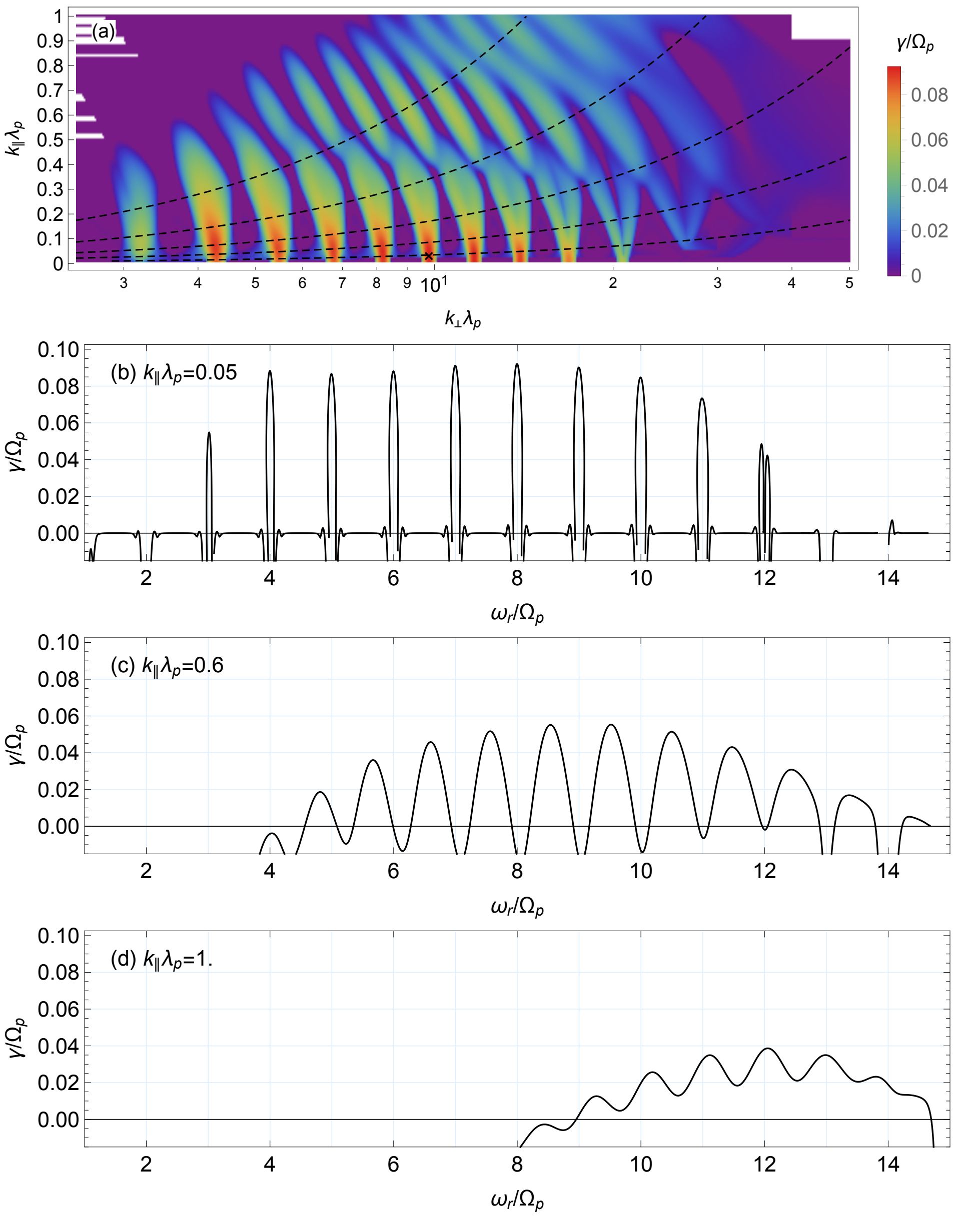

Figure S3. Linear theory results of the ion Bernstein instability for $m_p/m_e = 225$ and for Model 2 (see Table 1 in the article). The figure format is the same as Figure S2.

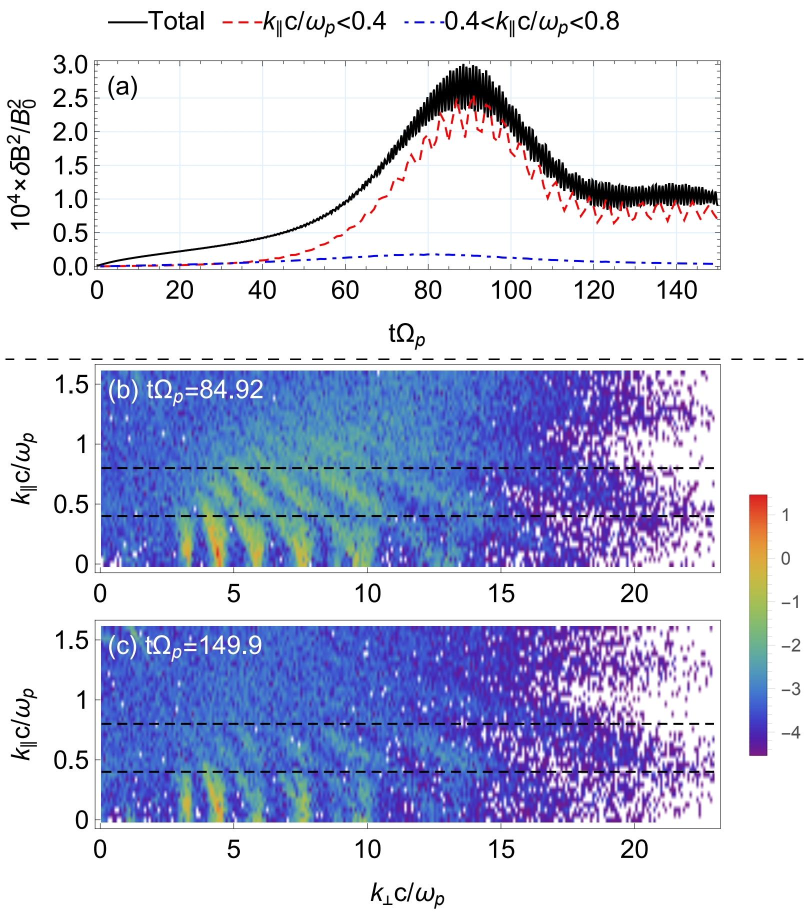

Figure S4. Summary plots of the PIC simulation with $m_p/m_e = 100$. (a) Time evolution of the total fluctuating magnetic field energy density (black solid), the energy density for the full harmonic modes in $|k_\parallel c/\omega_{pp}| \leq 0.4$ (red dashed), and the energy density for the half harmonic modes in $0.4 \leq |k_\parallel c/\omega_{pp}| \leq 0.8$ (blue dot-dashed). (b) Wave number spectrum of the fluctuating magnetic field ($|\delta\mathbf{B}|^2 = |\delta B_x|^2 + |\delta B_y|^2 + |\delta B_z|^2$) at $t\Omega_p \approx 85$. (c) Wave number spectrum of the fluctuating magnetic field at $t\Omega_p \approx 150$. The color scale is in a logarithmic scale, and the white patches in the spectra denote values less than the lower limit.

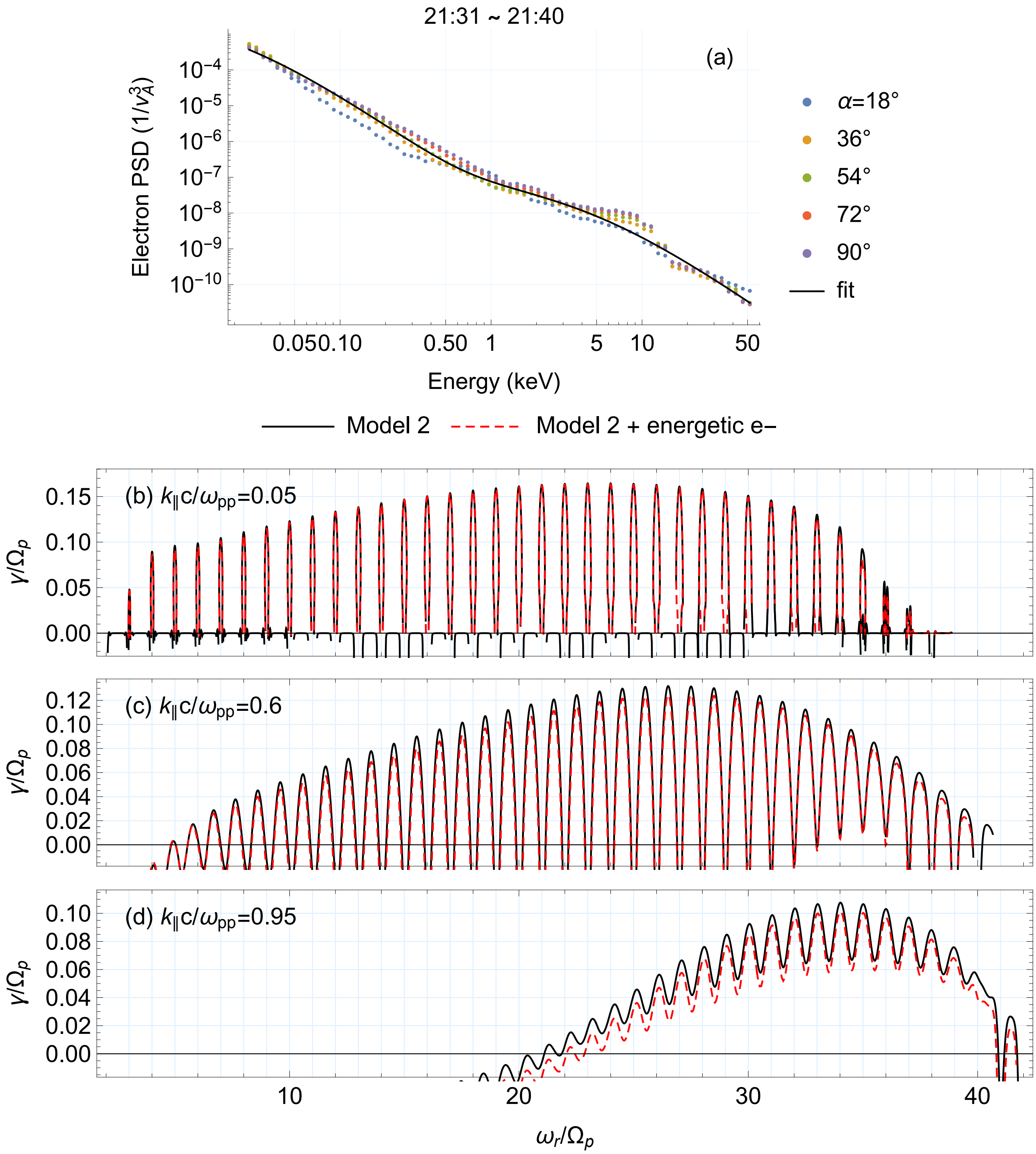

Figure S5. (a) Electron phase space density from the observation averaged between 2131 and 2140 UT (dots) and two-component kappa distribution fit (black curve). The colored dots correspond to different pitch angle bins as labeled. (b–d) Comparison of linear growth rates between proton Model 2 with the single Maxwellian model (black solid) and with the kappa model (red dashed) for $k_\parallel c/\omega_{pp} = 0.05$, 0.6 and 0.95, respectively.